

# Assessment of bilayer silicene to probe as quantum spin and valley Hall effect

Majeed Ur Rehman<sup>1,2,a</sup> and Zhenhua Qiao<sup>1,2</sup>

<sup>1</sup> ICQD, Hefei National Laboratory for Physical Sciences at Microscale, University of Science and Technology of China, Hefei, Anhui 230026, P.R. China

<sup>2</sup> CAS Key Laboratory of Strongly-Coupled Quantum Matter Physics, and Department of Physics, University of Science and Technology of China, Hefei 230026, P.R. China

Received 22 May 2017 / Received in final form 8 December 2017

Published online 19 February 2018 – © EDP Sciences, Società Italiana di Fisica, Springer-Verlag 2018

**Abstract.** Silicene takes precedence over graphene due to its buckling type structure and strong spin orbit coupling. Motivated by these properties, we study the silicene bilayer in the presence of applied perpendicular electric field and intrinsic spin orbit coupling to probe as quantum spin/valley Hall effect. Using analytical approach, we calculate the spin Chern-number of bilayer silicene and then compare it with monolayer silicene. We reveal that bilayer silicene hosts double spin Chern-number as compared to single layer silicene and therefore accordingly has twice as many edge states in contrast to single layer silicene. In addition, we investigate the combined effect of intrinsic spin orbit coupling and the external electric field, we find that bilayer silicene, likewise single layer silicene, goes through a phase transitions from a quantum spin Hall state to a quantum valley Hall state when the strength of the applied electric field exceeds the intrinsic spin orbit coupling strength. We believe that the results and outcomes obtained for bilayer silicene are experimentally more accessible as compared to bilayer graphene, because of strong SO coupling in bilayer silicene.

## 1 Introduction

Silicene has a honeycomb-structure, where the atoms of silicon are arranged in a buckled type manner [1,2]. The low energy physics of silicene has a close resemblance with the two dimensional (2D) massless Dirac spectrum [3] and therefore reasonably, the dynamics of electrons in silicene can be described by 2D massless Dirac equation instead of Schrodinger equation. It has been reported that silicene and its ribbons can be realized experimentally [4–6] by synthesis on metal surfaces. Silicene has many rich physical aspects in contrast to graphene because of its buckling type structure and strong intrinsic spin orbit (ISO) coupling and hence an intensive attention has been given to this new material, both experimentally and theoretically [1,4,6–14]. The energy spectrum of silicene can be gapped and controlled through the application of an external electric field [15,16] because of its buckling type structure, in this sense, it is considered to be a useful candidate for electronic devices. Unlike graphene, where the ISO interaction is weak, the quantum spin Hall effect (QSHE) can be observed experimentally in silicene because of having strong SOI [7]. More attention has been focused on this new topological phase QSHE from 2005 till now [17–24] because some new properties are believed to be extracted from it which could be useful for technological usage. In QSH state, materials exhibit insulating behavior in the

bulk and display conducting spin channels at the edges. These conducting edge channels are engineered in such a way that perturbations and impurities which respect TR symmetry cannot affect these channels because backscattering is prohibited [21,25–27] due to TR symmetry. The strong SO interaction in the materials has a key role to observe this new state of matter experimentally. Materials having the strong essence of SO interaction are supposed to play a vital role in the technological development of spintronics devices [17,28]. Another important state, analogous to QSH state, is the quantum valley Hall (QVH) effect [29–31], this phase originates as a result of inversion asymmetry in the system. The essential condition for  $Z_2$  topological phases is the preservation of TR symmetry in the system, in contrast, the key concept to have QVH effect is the absence of coupling between two valleys. The edge states in the QVH effect have valley-helical nature and are stable against perturbations and impurities that are smooth in nature. Unlike  $Z_2$  topological insulators, QVH states do not demand the strong spin orbit interaction to survive, its only requires the breaking of inversion symmetry in the system which can be done through the application of perpendicular electric field or substrate. The QVH effect could be useful to boost up the technology related to valleytronics. The band gap in topological insulator systems can be controlled through the application of electric field and in this sense electric field can be considered one of the efficient agent to derive a band insulator into the topological insulator. Such class

<sup>a</sup> e-mail: [majeedqau@live.com](mailto:majeedqau@live.com)

of topological insulators which is driven by the electric field are currently of great interest because of its potential device applications and fundamental physics [32–34].

Recently, the bilayer of silicene has been proposed experimentally [35] and a considerable attention has been paid to it [35–40]. Unlike the bilayer graphene where the two layers are connected through weak Van der Waals interactions, the two silicene sheets in bilayer silicene are attached through covalent-bonds to each other [41]. Our aim in this current manuscript is to analyze the topological future of bilayer silicene in the presence of ISO coupling and applied vertical electric field, using the two levels Hamiltonian approach. Likewise, the monolayer silicene which goes through a phase transition from a semimetallic to QSH state [15,16,31] when ISO coupling is introduced, in the similar fashion, the bilayer silicene also goes through a phase transition from metallic to a weak topological QSH state (also called quasi-topological state [37]). In addition, the band gap can be controlled by applying an electric field. Moreover, bilayer silicene goes through a phase transition from QSH state to a QVH state, when the strength of electric field exceeds the ISO coupling strength. Unlike the silicene monolayer, there is a probability of backscattering between the channels on a given edge moving in opposite directions with opposite spins, because unlike the monolayer silicene where edge state branches cross each other at the time reversal invariant momenta (TRIM), the edge state branches in bilayer silicene cross each other at the momenta which are not time reversal invariant. i.e. there is a crossing away from valley points and therefore the edge states in bilayer silicene are not protected by TR symmetry (Kramers theorem) [42]. Thus indeed, the edge states in bilayer silicene are not robust against perturbation that preserves TR symmetry and hence in this sense bilayer silicene belongs to the class of weak topological insulators. Weak topological insulators have an even number of Kramers pairs on a given edge and even smooth perturbations that respect TR symmetry (e.g. spin mixing perturbations) can destroy their gapless edge states [43]. In contrast, strong topological insulators have an odd number of Kramers pairs on a given edge and hence when one applies a perturbation that respects TR symmetry, at least one pair of gapless edge states will not be affected by this perturbation. Mathematically, strong and weak topological insulators are classified by  $Z_2$  topological invariant [42].

This manuscript is ordered as follow. In Section 2, we model the two bands Hamiltonian of bilayer silicene interms of three dimensional unit vector and calculate the spin-Chern/valley-Chern number. In Section 3, we encounter the possible effects due to trigonal warping on the quantum spin Hall effect. In Section 4, we model the two bands Hamiltonian of bilayer silicene (forward Bernal-stacking) in the presence of perpendicular electric field and discuss the interplay between the vertical electric field and ISO coupling strengths for the cases when Fermi level lies (i) inside the band gap and (ii) inside the conduction/valence band. In Section 4, we consider bilayer silicene (backward Bernal-stacking) and discuss the phase transition between QSH and QVH states. In Section 5, we summarize our results.

## 2 The model hamiltonian

The Bernal type stacking (AB stacking) of silicene bilayer has been reported to be thermodynamically stable among the possible arrangements [37]. In this type of stacking, atoms  $A_2$  of the top layer lie upon the  $B_1$  atoms of the bottom layer. Because of buckling nature, bilayer silicene possesses an extra degree of freedom in the sense how to stack the two silicene sheets, for instance forward and backwards Bernal-stacking types, these types have been discussed in detail in reference [37].

Irrespective of the type of stacking, the two-level effective Hamiltonian of bilayer silicene (Bernal stacking) in the basis  $\{\varphi_{A_1s_z}^\eta, \varphi_{B_2s_z}^\eta\}$ , can be written [37] as

$$\mathcal{H}_{s_z}^\eta(p) = \mathcal{H}_a + \mathcal{H}_b + \mathcal{H}_c, \quad (1)$$

where

$$\mathcal{H}_a = -\frac{v_F^2}{t_\perp} \begin{pmatrix} 0 & K_-^2 \\ K_+^2 & 0 \end{pmatrix}, \quad (2)$$

$$\mathcal{H}_b = -\frac{v_F^2}{t_\perp^2} \eta s_z \alpha_{so} \begin{pmatrix} K_- K_+ & 0 \\ 0 & -K_+ K_- \end{pmatrix}, \quad (3)$$

$$\mathcal{H}_c = -\eta s_z \alpha_{so} \sigma_z, \quad (4)$$

where  $K_+$  ( $K_-$ ) =  $p_x + ip_y$  ( $p_x - ip_y$ ),  $v_F$  [=  $(\sqrt{3}/2)at = 5 \times 10^5$  m/s] is the Fermi-velocity,  $a$  [=  $3.86 \text{ \AA}$ ] is the lattice-constant of monolayer silicene,  $t(t_\perp)$  describes the nearest neighbor intra layer (strong inter layer) coupling between  $A_j - B_j$  for  $j = 1, 2$  ( $B_1 - A_2$ ),  $\{\sigma_i, i = 0, 1, 2, 3\}$  represents the Pauli matrices in the  $A_1/B_2$  space,  $s_z$  [=  $\pm 1$ ] ( $\eta$  [=  $\pm 1$ ]) is the real spin (valley) index,  $\alpha_{so}$  is the strength of ISO interaction,  $\mathbf{p} = p[\cos \phi_p, \sin \phi_p]$  is the momentum and  $\phi_p = \tan^{-1}(p_y/p_x)$ . In this model the spin  $s_z$  is a good quantum-number.

The band structure for both valleys takes the form

$$E_n^{\eta, s_z}(p) = n \sqrt{\left(\frac{v_F^2 p^2}{t_\perp}\right)^2 + \left(-\eta s_z \alpha_{so} + \frac{\eta s_z \alpha_{so} v_F^2 p^2}{t_\perp}\right)^2} = n\lambda(p), \quad (5)$$

where

$$\lambda(p) = \left[ \left(\frac{v_F^2 p^2}{t_\perp}\right)^2 + \left(-\eta s_z \alpha_{so} + \eta s_z \alpha_{so} v_F^2 p^2 / t_\perp\right)^2 \right]^{1/2}, \quad (6)$$

and  $n$  [=  $\pm 1$ ] is the band index. It is quite visible from the above dispersion that the system becomes gaped when ISO interaction is taken into account. In addition, there exist spin degeneracy in the system which shows that the system is symmetric with respect to TR and space inversion symmetry. In order to look at, what kind of nature this insulator has; we calculate the spin Chern parity or winding number for the said system.

The Hamiltonian (1) can be set interms of 3D unit-vector  $\hat{N}(p)$  as

$$\mathcal{H}_{s_z}^\eta(p) = \lambda(p) \left[ \hat{N}_x(p)\sigma_x + \hat{N}_y(p)\sigma_y + \hat{N}_z(p)\sigma_z \right], \quad (7)$$

where the three-component unit-vector is defined as

$$\hat{N}(p) = \left[ -\delta(p) \cos(2\phi_p), -\eta\delta(p) \sin(2\phi_p), \hat{N}_z(p) \right], \quad (8)$$

where

$$\delta(p) = [1 - \hat{N}_z^2(p)]^{1/2}, \quad (9)$$

and

$$\hat{N}_z(p) = (-\eta s_z \alpha_{so} + \eta s_z \alpha_{so} v_F^2 p^2 / t_1) / \lambda(p). \quad (10)$$

The winding number interms of the unit-vector for the two band Hamiltonian (1) is documented [44] as

$$\mathbb{C}(\eta, s_z) = 1/4\pi \int dp_x dp_y F(p), \quad (11)$$

where

$$F(p) \equiv \left[ \left( \partial_p \hat{N}(p) \times \partial_p \hat{N}(p) \right) \cdot \hat{N}(p) \right]. \quad (12)$$

Physically, this number represent, how many times the 3D unit-vector  $\hat{N}(p)$  wind the whole unit sphere upon scanning the entire first B.Z. This number have a direct connection with the topology in the band structure and can possess different values for different band structures. The  $F(p)$  is a well-known quantity known as Berry curvature which is analogous to the magnetic field in electrodynamics and can be calculated as

$$F(p) = \xi_I + \xi_{II} + \xi_{III}, \quad (13)$$

with

$$\xi_I = -\frac{2\eta}{p} \cos^2 2\phi_p \delta(p) \partial_p \hat{N}_z(p), \quad (14)$$

$$\xi_{II} = -\frac{2\eta}{p} \sin^2 2\phi_p \delta(p) \partial_p \hat{N}_z(p), \quad (15)$$

and

$$\xi_{III} = -\frac{2\eta}{p} \hat{N}_z^2(p) \partial_p \hat{N}_z(p), \quad (16)$$

where we have used

$$\begin{aligned} \partial_{p_x} \hat{N}_x(p) &= -2 \sin(3\phi_p) \delta(p) \beta_1 - p \cos(2\phi_p) \partial_p \delta(p) \beta_2, \\ \partial_{p_y} \hat{N}_x(p) &= 2 \sin(\phi_p) \delta(p) \beta_2 - p \cos(2\phi_p) \partial_p \delta(p) \beta_1, \end{aligned}$$

$$\begin{aligned} \partial_{p_x} \hat{N}_y(p) &= 2\eta \cos(2\phi_p) \delta(p) \beta_1 - \eta p \sin(2\phi_p) \partial_p \delta(p) \beta_2, \\ \partial_{p_y} \hat{N}_y(p) &= -2\eta \cos(2\phi_p) \delta(p) \beta_2 - \eta p \sin(2\phi_p) \partial_p \delta(p) \beta_1, \end{aligned}$$

$$\begin{aligned} \partial_{p_x} \hat{N}_z(p) &= \partial_p \hat{N}_z(p) \cdot p \beta_2, \text{ and } \partial_{p_y} \hat{N}_z(p) = \partial_p \hat{N}_z(p) \cdot p \beta_1, \\ \partial_{p_x} \phi_p &= -\beta_1, \partial_{p_y} \phi_p = -\beta_2, \partial_{p_x} p = p \beta_2 \partial_p, \\ \partial_{p_y} p &= p \beta_1 \partial_p, \beta_{1(2)} = p_{y(x)} / p^2, \end{aligned}$$

now, we substitute equation (13) into equation (11)

$$\mathbb{C}(\eta, s_z) = \frac{-\eta}{2\pi} \int_0^\infty \int_0^{2\pi} p dp d\phi \frac{1}{p} \partial_p \hat{N}_z(p), \quad (17)$$

$$\mathbb{C}(\eta, s_z) = \eta \hat{N}_z(0) = -s_z. \quad (18)$$

The total Chern-number can be calculated as

$$\mathcal{C} = \sum_{\eta=\pm 1} \sum_{s_z=\pm 1} (\mathbb{C}(\eta, s_z)) = 0. \quad (19)$$

This ensures the TR symmetry in the system, additionally, there is no electric current flowing. Another interesting result can also be seen that the Chern-number gets quantized when the contribution from both valleys are considered, which justify the statement that each filled band cannot have a fractional value of the Chern-number [45].

$$\mathcal{C}_\uparrow = \sum_{\eta=\pm 1} (\mathbb{C}(\eta, \uparrow)) = -2, \quad \mathcal{C}_\downarrow = \sum_{\eta=\pm 1} (\mathbb{C}(\eta, \downarrow)) = 2. \quad (20)$$

The spin Chern-number/Chern parity is a topological index used to classify systems having spin-rotational symmetry and can be defined in the following manner [17,23,46,47],

$$\mathcal{C}_s = \sum_{i \in \text{occ}} \left( \frac{\mathbb{C}_\uparrow^{(i)} - \mathbb{C}_\downarrow^{(i)}}{2} \right), \quad (21)$$

where the summation goes through over the occupied-bands. Thus the spin Chern parity for our bilayer silicene system is  $\mathcal{C}_s = [(\mathcal{C}_\uparrow - \mathcal{C}_\downarrow) / 2] = -2$ , and the corresponding spin Hall conductivity is

$$\sigma_{xy}^s (\text{spin}) \left[ = \mathcal{C}_s \frac{e^2}{h} \right] = -2 \frac{e^2}{h}. \quad (22)$$

From this, it is quite crystal that spin Chern-number of bilayer silicene is double than that of a single layer silicene and therefore have twice as many edge states as that of single layer of silicene. The valley Chern number is zero, which shows that there is no valley Hall effect in

**Table 1.** Topological configuration of bilayer silicene with associated topological charges.

Flavours	Vortex core	Asymptotically large momentum	$\mathbb{C}(\eta, s_z)$	Topological structure
$(\mathbb{K}, \uparrow)$	$\hat{\mathbb{N}} = (0, 0, -1)$	$\hat{\mathbb{N}} = (-\cos 2\varphi, -\sin 2\varphi, 0)$	-1	Double-vortex meron
$(\mathbb{K}', \uparrow)$	$\hat{\mathbb{N}} = (0, 0, 1)$	$\hat{\mathbb{N}} = (-\cos 2\varphi, \sin 2\varphi, 0)$	-1	Double-vortex meron
$(\mathbb{K}, \downarrow)$	$\hat{\mathbb{N}} = (0, 0, 1)$	$\hat{\mathbb{N}} = (-\cos 2\varphi, -\sin 2\varphi, 0)$	1	Double-vortex anti-meron
$(\mathbb{K}', \downarrow)$	$\hat{\mathbb{N}} = (0, 0, -1)$	$\hat{\mathbb{N}} = (-\cos 2\varphi, \sin 2\varphi, 0)$	1	Double-vortex anti-meron

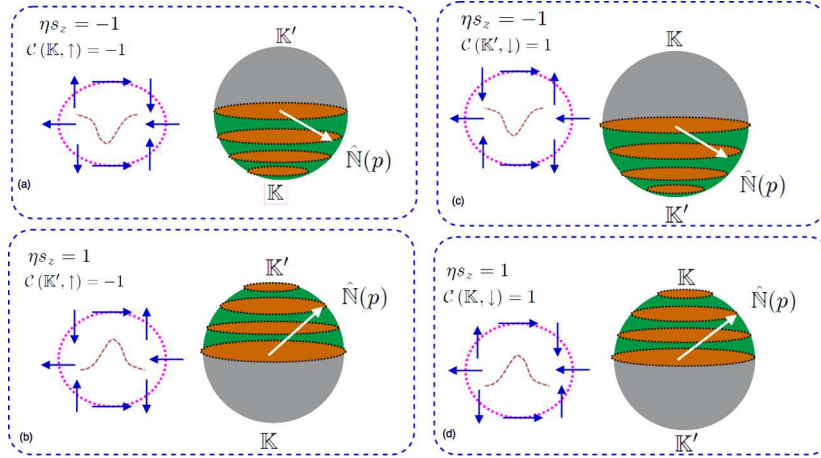


**Fig. 1.** Four branches of double-vortex merons. (a) Branch with valley  $\mathbb{K}$  and  $\uparrow$ : the unit vector  $\hat{\mathbb{N}}(p)$  covers lower hemi sphere and display double vortex meron like configuration with associated topological charge  $\mathcal{C}(\mathbb{K}, \uparrow) = -1$ . (b) Branch with valley  $\mathbb{K}'$  and  $\uparrow$ :  $\hat{\mathbb{N}}(p)$  covers upper hemisphere and display double-vortex meron like structure with  $\mathcal{C}(\mathbb{K}', \uparrow) = -1$ . (c) Flavour with valley  $\mathbb{K}'$  and  $\downarrow$ : the mapping  $\hat{\mathbb{N}}(p)$  covers lower hemi sphere and display double-vortex anti-meron like configuration with associated topological charge  $\mathcal{C}(\mathbb{K}', \downarrow) = 1$ . (d) Flavour with valley  $\mathbb{K}$  and  $\downarrow$ :  $\hat{\mathbb{N}}(p)$  covers upper hemisphere and display double-vortex anti-meron like structure  $\mathcal{C}(\mathbb{K}, \downarrow) = 1$ .

the bilayer silicene system.

$$\mathcal{C}_v = \sum_{s_z = \pm 1} \frac{1}{2} [\mathcal{C}(\mathbb{K}, s_z) - \mathcal{C}(\mathbb{K}', s_z)] = 0. \quad (23)$$

### 3 Topological structure

The topological structure of bilayer silicene can be seen by mapping the 3D unit vector  $\hat{\mathbb{N}}(p)$  over the 3D unit sphere. We observe that bilayer silicene displays double vortex merons like configuration [see Fig. 1]. In contrast to single layer silicene, the mapping  $\hat{\mathbb{N}}(p)$  covers the 3D unit sphere twice, upon scanning the entire B.Z. In principle, here we have four branches  $\{(\mathbb{K}, \uparrow), (\mathbb{K}', \uparrow), (\mathbb{K}, \downarrow), (\mathbb{K}', \downarrow)\}$ . The topological structure of these branches is well explained in Table 1.

see Table 1 at the top of this page.

It is interesting to note that although these topological objects have twice the topological charge as that of a meron (half of skyrmion), however, in fact, these objects are not skyrmions because of different nature at asymptotically large momentum and hence given the name as *double-vortex merons*.

### 4 Trigonal warping effects

In order to encounter the possible effects due to trigonal warping on the quantum spin Hall effect in bilayer silicene, we incorporate the trigonal warping term in the Hamiltonian (1). By involving the trigonal effects the Hamiltonian (1) takes the form

$$\mathcal{H}_{s_z}^n = \mathcal{H}_a + \mathcal{H}_b + \mathcal{H}_c + \mathcal{H}_d, \quad (24)$$

where the trigonal term is

$$\mathcal{H}_d = \eta v_3 \begin{pmatrix} 0 & K_+ \\ K_- & 0 \end{pmatrix}. \quad (25)$$

Here  $v_3 = (\sqrt{3/2})at_3/\hbar$  with  $t_3$  represent coupling between B1 and A1 sites. By diagonalizing the above Hamiltonian, we get

see equation (26) next page

In the limit  $v_3 \rightarrow 0$ , we recover the same situation as without trigonal effects [Eq. (5)]. In the absence of intrinsic SO coupling and this new (trigonal) term in the Hamiltonian, the observed spectrum is quadratically isotropic displaying circular Fermi lines around the valley point's  $\mathbb{K}$  and  $\mathbb{K}'$ , and when one switched on the intrinsic

$$E_n^{\eta, s_z} = n \sqrt{\left(\frac{v_F^2 p^2}{t_\perp}\right)^2 + v_3^2 p^2 + \frac{v_F^2 \eta v_3 p^3}{t_\perp} \cos 3\varphi + \left(-\eta s_z \alpha_{\text{SO}} + \frac{\eta s_z \alpha_{\text{SO}} v_F^2 p^2}{t_\perp}\right)^2} \quad (26)$$

SO coupling alone, a gap is opened at both these valley points. Now when this new term is introduced in the Hamiltonian with zero intrinsic SO coupling, it stretches the iso-energy lines in three different directions (as cleared from the dispersion relation), that is the Dirac points  $\mathbb{K}$  and  $\mathbb{K}'$  split into three more Dirac points where conduction and valence band touch each other. One Dirac point is at the centre (zero momentum) while the other three lies at some finite momenta in the direction of  $\phi$ . Now when we also switched on the intrinsic SO coupling the energy gap is opened at these four Dirac points with each one contributing in such a way to make the spin Chern number equal to the case with no trigonal effects.

The Hamiltonian (24) can be parametrized in terms of 3D unit vector  $\hat{\mathbf{N}}(p)$  as

$$\mathcal{H}_{s_z}^\eta = \sum_{i=x,y,z} \sigma_i \hat{N}_i(p), \quad (27)$$

where

$$\hat{N}_x(p) = \eta v_3 p \cos \phi_p + (\eta v_3^3 p^3 / t_\perp^2) \cos(3\phi_p), \quad (28)$$

$$\hat{N}_y(p) = -\eta v_3 p \sin \phi_p + (v_3^3 p^3 / t_\perp^2) \sin(3\phi_p), \quad (29)$$

and

$$\hat{N}_z(p) = \alpha_{\text{SO}} \eta s_z. \quad (30)$$

Using equation (11), we get the same spin Chern-number as in Section 2 i.e.  $C_s = -2$ . This shows that trigonal effects, like graphene bilayer, do not affect the spin Chern-number. In principle, all the newly designed Dirac points due to trigonal warping, equally contribute in the spin Chern number to make it quantify with a value equal to the case with no trigonal effects.

## 5 Model Hamiltonian in the presence of perpendicular electric field

In principle, there are two types of stacking in bilayer silicene, one is called forward Bernal-stacking and other is backward Bernal-stacking (for more details, see Ref. [37]). We first consider the forward Bernal stacking case.

### 5.1 Forward Bernal-stacking ( $B_2A_2 - B_1A_1$ type)

The two band Hamiltonian of bilayer silicene ( $B_2A_2 - B_1A_1$  type stacking) in the presence of perpendicular electric field in the basis  $\{\varphi_{A_1s_z}^\eta, \varphi_{B_2s_z}^\eta\}$ , can be modelled as [37]

$$\mathcal{H}_{s_z}^\eta = \mathcal{H}_a + \mathcal{H}_b + \mathcal{H}_c + \mathcal{H}_{E_Z}, \quad (31)$$

$$\mathcal{H}_a = -\frac{v_F^2}{t_\perp} \begin{pmatrix} 0 & K_-^2 \\ K_+^2 & 0 \end{pmatrix}, \quad (32)$$

where

$$\mathcal{H}_b = -\frac{v_F^2}{t_\perp^2} \eta s_z \alpha_{\text{SO}} \begin{pmatrix} K_- K_+ & 0 \\ 0 & -K_+ K_- \end{pmatrix}, \quad (33)$$

$$\mathcal{H}_c = -\eta s_z \alpha_{\text{SO}} \sigma_z, \quad (34)$$

$$\mathcal{H}_{E_Z} = \Delta_{z_1} \sigma_z - \frac{v_F^2}{t_\perp^2} \Delta_{z_2} \begin{pmatrix} K_- K_+ & 0 \\ 0 & -K_+ K_- \end{pmatrix}. \quad (35)$$

Here,  $\Delta_{z_1} \equiv (L - l)E_Z$  and  $\Delta_{z_2} \equiv (L + l)E_Z$ , with  $l$  represents the separation between the two sublattice planes as silicene has buckled type structure while  $L$  represents the interlayers separation. This Hamiltonian can be diagonalized as

see equation (36) next page

where

$$\varepsilon(p) = \left[ \left( \frac{v_F^2 p^2}{t_\perp} \right)^2 + (\Delta_{z_1} - \eta s_z \alpha_{\text{SO}} - \left( \frac{v_F^2 p^2}{t_\perp} \right) (\Delta_{z_2} + \eta s_z \alpha_{\text{SO}}))^2 \right]^{1/2}, \quad (37)$$

and  $n [= \pm 1]$  is the band index with  $+1(-1)$  represents conduction (valence) band.

We see that there is an interesting interplay exist between the applied electric field and ISO coupling strength which can be summarized as: (i) when one of both  $\alpha_{\text{SO}}$  and  $\Delta_{z_1}$  is non-zero, we have a gaped spectrum with no spin splitting [see Fig. 2a]. (ii) When both are non-zero such that  $\alpha_{\text{SO}} > \Delta_{z_1} > 0$ , spin degeneracy lift in the sense that spin- $\uparrow$  ( $\downarrow$ ) bands moves downward (upward) due to the inversion asymmetry and electric field is responsible for this, the system stays as a topological insulator with gapless edge states [see Fig. 2b]. (iii) The gap between the spin-up bands gets decreases when the value of electric field increases and completely vanishes at the valley points when both  $\alpha_{\text{SO}}$  and  $\Delta_{z_1}$  become equal in magnitude [see Fig. 2c]. (iv) When the value of electric field further increases i.e.,  $\Delta_{z_1} > \alpha_{\text{SO}} > 0$ , the gap reopens corresponding to a phase transition from a QSH state to QVH state [see Fig. 2d]. One more thing that needs to be included in the discussion is the energy gap between valence and conduction band, the energy gap at the valley points is  $\Delta_g = 2(\alpha_{\text{SO}} - \Delta_{z_1})$ . Our system remains gaped as long as  $\Delta_g \neq 0$  and one can determine unambiguously the spin

$$E_n^{\eta, s_z}(p) = n\sqrt{\left(\frac{v_F^2 p^2}{t_1}\right)^2 + \left(\Delta z_1 - \eta s_z \alpha_{SO} - \frac{v_F^2 p^2}{t_1^2} (\Delta z_2 + \eta s_z \alpha_{SO})\right)^2} = n\varepsilon(p) \quad (36)$$

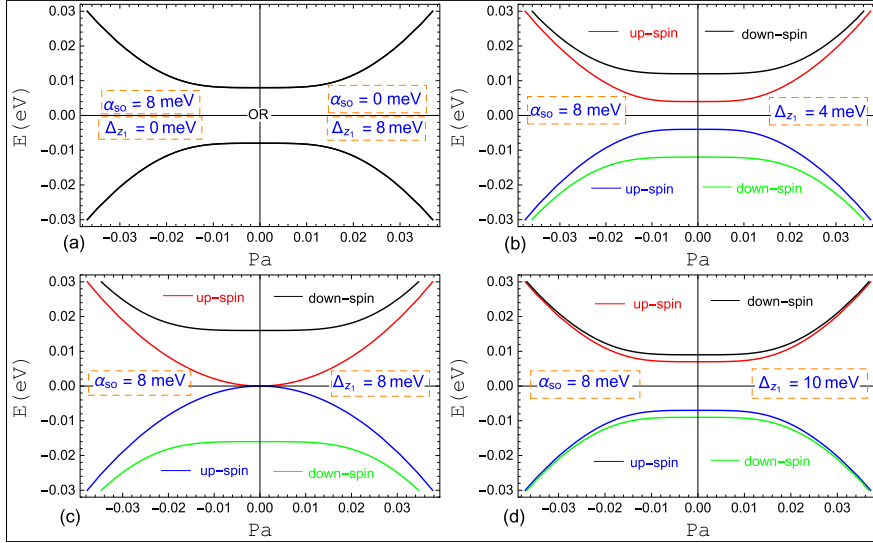


**Fig. 2.** Band structure of bilayer silicene for different values of electric field and ISO coupling. Different values of  $\Delta z_1$  and  $\alpha_{SO}$  are mentioned inside the plots.

Chern-number. The Hamiltonian (31) can be modelled interms of 3D unit vector  $\hat{N}(p)$  as

$$\mathcal{H}_{s_z}^{\eta}(p) = \varepsilon(p) \left[ \hat{N}_x(p)\sigma_x + \hat{N}_y(p)\sigma_y + \hat{N}_z(p)\sigma_z \right], \quad (38)$$

where the three-component unit  $\hat{N}(p)$  vector is defined as

$$\hat{N}(p) = \left[ -\delta(p) \cos(2\phi_p), -\eta\delta(p) \sin(2\phi_p), \hat{N}_z(p) \right], \quad (39)$$

where

$$\delta(p) = [1 - \hat{N}_z^2(p)]^{1/2}, \quad (40)$$

and

$$\hat{N}_z(p) = \frac{[\Delta z_1 - \eta s_z \alpha_{SO} - (v_F^2 p^2 / t_1) (\Delta z_2 + \eta s_z \alpha_{SO})]}{\varepsilon(p)}. \quad (41)$$

Repeating the same process as we did in Section 2, we get

$$\mathcal{C}(\eta, s_z) = \eta \hat{N}_z(0) = \eta \text{sgn}(\Delta z_1 - \eta s_z \alpha_{SO}). \quad (42)$$

Hence we find

$$\mathcal{C} = \sum_{\eta=\pm 1} [\mathcal{C}(\eta, \uparrow) + \mathcal{C}(\eta, \downarrow)] = 0, \quad (43)$$

$$\begin{aligned} \mathcal{C}_s = \sum_{\eta=\pm 1} \frac{1}{2} [\mathcal{C}(\eta, \uparrow) - \mathcal{C}(\eta, \downarrow)] = & -[\text{sgn}(\alpha_{SO} + \Delta z_1) \\ & + \text{sgn}(\alpha_{SO} - \Delta z_1)], \end{aligned} \quad (44)$$

$$\begin{aligned} \mathcal{C}_v = \sum_{s_z=\pm 1} \frac{1}{2} [\mathcal{C}(\mathbb{K}, s_z) - \mathcal{C}(\mathbb{K}', s_z)] = & [\text{sgn}(\alpha_{SO} + \Delta z_1) \\ & - \text{sgn}(\alpha_{SO} - \Delta z_1)]. \end{aligned} \quad (45)$$

And the corresponding spin/valley Hall conductivities is given as

$$\begin{aligned} \sigma_{xy}(\text{spin}) = \mathcal{C}_s \frac{e^2}{h} = & -\frac{e^2}{h} [\text{sgn}(\alpha_{SO} + \Delta z_1) \\ & + \text{sgn}(\alpha_{SO} - \Delta z_1)], \end{aligned} \quad (46)$$

$$\begin{aligned} \sigma_{xy}(\text{valley}) = \mathcal{C}_v \frac{e^2}{h} = & \frac{e^2}{h} [\text{sgn}(\alpha_{SO} + \Delta z_1) \\ & - \text{sgn}(\alpha_{SO} - \Delta z_1)]. \end{aligned} \quad (47)$$

It is quite evident from these equations that bilayer silicene exhibits (i) QSH state with  $\sigma_{xy}^s(\text{spin}) = -2e^2/h$  and  $\sigma_{xy}^s(\text{valley}) = 0$ , for the case  $\alpha_{SO} > \Delta z_1 > 0$ . (ii) QVH state  $\sigma_{xy}^s(\text{spin}) = 0$  and  $\sigma_{xy}^s(\text{valley}) = -2e^2/h$ , for the

case  $\Delta z_1 > \alpha_{so} > 0$ . Despite the fact that we have considered the Fermi-level inside the energy-gap between the conduction and valence bands, still we have the conductivity in the system which is a clear justification of the statement that system under consideration has gapless edge states and these gapless states are responsible for this finite conductivity.

Now taking into account a more realistic situation where the Fermi-level lies in one of the band i.e., in conduction-band or valence-band. So when the Fermi-level lies in the conduction-band, we have

$$\mathbb{C}(\eta, s_z) = \frac{-\eta}{2\pi} \int_0^{p_F} \int_0^{2\pi} p dp d\phi \frac{1}{p} \partial_p \hat{N}_z(p), \quad (48)$$

$$\mathbb{C}(\eta, s_z) = -\eta [\hat{N}_z(p_F) - \hat{N}_z(0)], \quad (49)$$

$$= -\eta \left[ \text{sign}(\eta s_z \alpha_{so} - \Delta z_1) - \hat{N}_z(p_F) \right], \quad (50)$$

with

$$\hat{N}_z(p_F) = \frac{\Delta z_1 - \eta s_z \alpha_{so} - (v_F^2 p_F^2 / t_1) (\Delta z_2 + \eta s_z \alpha_{so})}{\varepsilon(p_F)}. \quad (51)$$

The spin Chern number becomes

$$\mathcal{C}_s = \Pi_1(p_F) - \Pi_2(p_F), \quad (52)$$

with

$$\Pi_1(p_F) = \frac{-(\alpha_{so} + \Delta z_1) + \kappa_1}{\sqrt{(v_F^2 p_F^2 / t_\perp^2)^2 + (\Delta z_1 + \alpha_{so} - \kappa_1)^2}}, \quad (53)$$

$$\Pi_2(p_F) = \frac{\alpha_{so} - \Delta z_1 + \kappa_2}{\sqrt{(v_F^2 p_F^2 / t_\perp^2)^2 + (\Delta z_1 - \alpha_{so} - \kappa_2)^2}},$$

where

$$\kappa_1 = (v_F^2 p_F^2 / t_1^2) (\Delta z_2 - \alpha_{so}), \quad (54)$$

and

$$\kappa_2 = (v_F^2 p_F^2 / t_1^2) (\Delta z_2 + \alpha_{so}). \quad (55)$$

And the corresponding spin conductivity then becomes

$$\sigma_{xy}^F(\text{spin}) = [\Pi_1(p_F) - \Pi_2(p_F)] \frac{e^2}{h}. \quad (56)$$

In the same way, we get valley Chern number and its related conductivity as

$$\mathcal{C}_v = [\Pi_1(p_F) + \Pi_2(p_F)], \quad (57)$$

$$\sigma_{xy}^F(\text{valley}) = [\Pi_1(p_F) + \Pi_2(p_F)] \frac{e^2}{h}. \quad (58)$$

These expressions show that bilayer silicene goes through a phase-transition from QSH to a QVH state in a similar way as of the case where the Fermi-level lies inside the gap. The same results are obtained, when the Fermi-level lies inside valence-band because the system under consideration has the electron-hole symmetry. The spin/valley Hall conductivity is plotted in Figure 3 against applied electric field for both the cases when Fermi-level is in the (i) conduction or valence-band and (ii) energy gap.

## 5.2 Backward Bernal-stacking ( $B_2A_2 - A_1B_1$ and $A_2B_2 - B_1A_1$ types)

The backward Bernal-stacking of the types  $B_2A_2 - A_1B_1$  and  $A_2B_2 - B_1A_1$  are, in principle, identical [37]. The low energy two bands Hamiltonian for the backward Bernal-stacking takes the form [37]

$$\mathcal{H}_{s_z}^\eta = \mathcal{H}_a + \mathcal{H}_b + \mathcal{H}_c + \mathcal{H}_{E_Z}, \quad (59)$$

where

$$\mathcal{H}_a = -\frac{v_F^2}{t_\perp} \begin{pmatrix} 0 & K_-^2 \\ K_+^2 & 0 \end{pmatrix}, \quad (60)$$

$$\mathcal{H}_b = -\frac{v_F^2}{t_\perp^2} \eta s_z \alpha_{so} \begin{pmatrix} K_- K_+ & 0 \\ 0 & -K_+ K_- \end{pmatrix}, \quad (61)$$

$$\mathcal{H}_c = -\eta s_z \alpha_{so} \sigma_z, \quad (62)$$

$$\mathcal{H}_{E_Z} = \Delta z_3 \sigma_z - \Delta z_4 \begin{pmatrix} 1 & 0 \\ 0 & 1 \end{pmatrix} + \frac{v_F^2}{t_\perp^2} \Delta z_4 \begin{pmatrix} K_- K_+ & 0 \\ 0 & K_+ K_- \end{pmatrix} - \frac{v_F^2}{t_\perp^2} \Delta z_3 \begin{pmatrix} K_- K_+ & 0 \\ 0 & -K_+ K_- \end{pmatrix}. \quad (63)$$

Here,  $\Delta z_3 \equiv LE_Z$  and  $\Delta z_4 \equiv lE_Z$ . This Hamiltonian can be diagonalized as

*see equation (64) next page*

where  $n[=\pm 1]$  is the band index with  $+1(-1)$  represents conduction (valence) band. The energy gap at the valley points, in this case, is  $\Delta_g = 2\alpha_{so} - 2\Delta z_3$ .

The Hamiltonian (59) can be parametrized interms of 3D unit vector  $\hat{N}(p)$  as

$$\mathcal{H}_{s_z}^\eta = \epsilon(p) \sigma_0 + \sum_{i=x,y,z} \sigma_i \hat{N}_i(p), \quad (65)$$

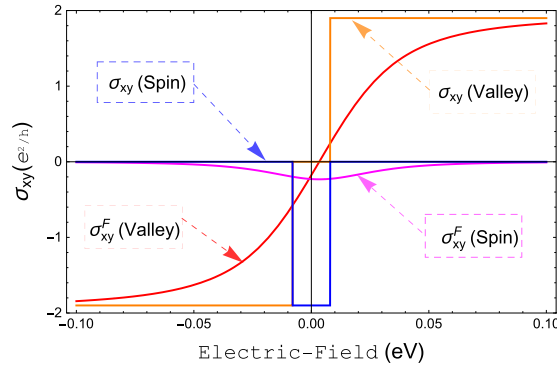


**Fig. 3.** Quantum spin/valley Hall conductivities as a function of applied electric-field for a fixed value of ISO coupling (4 meV).

$$E_n^{\eta, s_z}(p) = \frac{\Delta_{z4} v_F^2 p^2}{t_1^2} + n \sqrt{\left( \frac{v_F^2 p^2}{t_1} \right)^2 + \left( \Delta_{z3} - \eta s_z \alpha_{SO} - \frac{v_F^2 p^2}{t_1^2} (\Delta_{z3} + \eta s_z \alpha_{SO}) \right)^2} \quad (64)$$

where  $\epsilon(p) = \gamma(p) \Delta_{z4}$  with  $\gamma(p) = (1 + \hbar^2 v_F^2 p^2 / t_1^2)$ , and

$$\hat{N}_x(p) = -\delta(p) \cos(2\phi_p), \quad (66)$$

$$\hat{N}_y(p) = -\eta \delta(p) \sin(2\phi_p), \quad (67)$$

$$\hat{N}_z(p) = \Delta_{z3} - \eta s_z \alpha_{SO} - (v_F^2 p^2 / t_1^2) (\Delta_{z3} + \eta s_z \alpha_{SO}). \quad (68)$$

Using equation (11), we find

$$\sigma_{xy}(\text{spin}) = C_s \frac{e^2}{h} = -\frac{e^2}{h} [sgn(\alpha_{SO} + \Delta_{z3}) + sgn(\alpha_{SO} - \Delta_{z3})], \quad (69)$$

$$\sigma_{xy}(\text{valley}) = C_v \frac{e^2}{h} = \frac{e^2}{h} [sgn(\alpha_{SO} + \Delta_{z3}) - sgn(\alpha_{SO} - \Delta_{z3})]. \quad (70)$$

The energy gap at the valley points, in this case, is  $\Delta_g = 2(\alpha_{SO} - \Delta_{z3})$ . When  $\alpha_{SO} > \Delta_{z3} > 0$ , bilayer silicene stays as QSH state, show metallic behavior when  $\alpha_{SO} = \Delta_{z3}$  and make transition into QVH state when  $\Delta_{z3} > \alpha_{SO} > 0$ .

## 6 Summary

In conclusion, bilayer silicene favour to be in QSH state when ISO interaction is introduced, in addition, it makes a transition from QSH state to a QVH state when the strength of applied electric field exceeds the ISO coupling strength. The spectrum of bilayer silicene shows metallic behavior when the magnitude of the electric field becomes equal to the ISO coupling strength. The results in this paper show that spin splitting in bilayer silicene systems can be controlled by the application of electric

field or gate-voltage. This aspect of bilayer silicene makes its crucial for spintronics devices.

The author Majeed Ur Rehman, acknowledges the support from the Chinese Academy of Sciences (CAS) and TWAS for his PhD studies at the University of Science and Technology of China in the category of 2016 CAS-TWAS President's Fellowship Awardee (Series No. 2016-156). We also acknowledge the financial support from National Natural Science Foundation of China (NNSFC, Grant No.11474265) for the completion of this work.

## Author contribution statement

Majeed Ur Rehman performed all the calculations. All the authors interpreted physics, discussed the results and contributed to the writing of the paper. All authors reviewed the manuscript. Zhenhua Qiao supervised the whole work.

## References

1. K. Takeda, K. Shiraishi, Phys. Rev. B **50**, 14916 (1994)
2. G.G. Guzman-Verri, L.C. Lew Yan Voon, Phys. Rev. B **76**, 075131 (2007)
3. P. Vogt, P.D. Padova, C. Quaresima, J. Avila, E. Frantzeskakis, M.C. Asensio, A. Resta, B. Ealet, G.L. Lay, Phys. Rev. Lett. **108**, 155501 (2012)
4. B. Lalmi, H. Oughaddou, H. Enriquez, A. Kara, S. Vizzini, B. Ealet, B. Aufray, Appl. Phys. Lett. **97**, 223109 (2010)
5. B. Aufray, A. Kara, S. Vizzini, H. Oughaddou, C. Leandri, B. Ealet, G.L. Lay, Appl. Phys. Lett. **96**, 183102 (2010)
6. P.E. Padova, C. Quaresima, C. Ottaviani, P.M. Sheverdyeva, P. Moras, C. Carbone, D. Topwal, B. Olivieri, A. Kara, H. Oughaddou, B. Aufray, G.L. Lay, Appl. Phys. Lett. **96**, 261905 (2010)
7. K. Takeda, K. Shiraishi, Phys. Rev. B **50**, 075131 (1994)
8. S. Cahangirov, M. Topsakal, E. Akturk, H. Sahin, S. Ciraci, Phys. Rev. Lett. **102**, 236804 (2009)
9. C.-C. Liu, W. Feng, Y. Yao, Phys. Rev. Lett. **107**, 076802 (2011)

10. Y. Ding, J. Ni, Appl. Phys. Lett. **95**, 083115 (2009)
11. R. Qin, C.-H. Wang, W. Zhu, Y. Zhang, AIP Adv. **2**, 022159 (2012)
12. Y. Ding, Y. Wang, Appl. Phys. Lett. **100**, 083102 (2012)
13. C.H. Pan, Z. Li, C.C. Liu, G. Zhu, Z. Qiao, Y. Yao, Phys. Rev. Lett. **112**, 106802 (2014)
14. Y. Ren, Z. Qiao, Q. Niu, Rep. Prog. Phys. **79**, 066501 (2016)
15. M. Ezawa, New J. Phys. **14**, 033003 (2012)
16. M. Ezawaa, Eur. Phys. J. B **85**, 363 (2012)
17. C.L. Kane, E.J. Mele, Phys. Rev. Lett. **95**, 226801 (2005)
18. Y.G. Yao, F. Ye, X.L. Qi, S.C. Zhang, Z. Fang, Phys. Rev. B **75**, 041401(R) (2007)
19. D. Huertas-Hernando, F. Guinea, A. Brataas, Phys. Rev. B **74**, 155426 (2006)
20. H. Min, J.E. Hill, N.A. Sinitsyn, B.R. Sahu, L. Kleinman, A.H. MacDonald, Phys. Rev. B **74**, 165310 (2006)
21. C.L. Kane, E.J. Mele, Phys. Rev. Lett. **95**, 146802 (2005)
22. B.A. Bernevig, T.L. Hughes, S.C. Zhang, Science **314**, 1757 (2006)
23. H. Li, L. Sheng, D.Y. Xing, Phys. Rev. Lett. **108**, 196806 (2012)
24. M.U. Rehman, A.A. Abid, Chin. Phys. B **26**, 127304 (2017)
25. G. Tkachova, M. Hentschel, Eur. Phys. J. B **69**, 499 (2009)
26. M.Z. Hasan, S.-Y. Xu, G. Bian, Phys. Scr. **T164**, 014001 (2015)
27. T. Neupert, C. Chamon, T. Iadecola, L.H. Santos, C. Mudry, Phys. Scr. **T164**, 014005 (2015)
28. D. Pesin, A.H. MacDonald, Nat. Mater. **11**, 409 (2012)
29. D. Xiao, W. Yao, Q. Niu, Phys. Rev. Lett. **99**, 236809 (2007)
30. A. Rycerz, J. Tworzydło, C.W.J. Beenakker, Nat. Phys. **3**, 172 (2007)
31. M. Tahir, A. Manchon, K. Sabeeh, U. Schwingenschlogl, Appl. Phys. Lett. **102**, 162412 (2013)
32. J. Li, K. Chang, Appl. Phys. Lett. **95**, 222110 (2009)
33. M.S. Miao, Q. Yan, C.G. Van de Walle, W.K. Lou, L.L. Li, K. Chang, Phys. Rev. Lett. **109**, 186803 (2012)
34. D. Zhang, W. Lou, M. Miao, S.-C. Zhang, K. Chang, Phys. Rev. Lett. **111**, 156402 (2013)
35. B. Feng, Z. Ding, S. Meng, Y. Yao, X. He, P. Cheng, L. Chen, K. Wu, Nano Lett. **12**, 3507 (2012)
36. C. Lian, J. Niu, AIP Adv. **3**, 052102 (2013)
37. M. Ezawa, J. Phys. Soc. Jpn **81**, 104713 (2012)
38. H. Da, W. Ding, X. Yan, Appl. Phys. Lett. **110**, 141105 (2017)
39. H. Fu, J. Zhang, Z. Ding, H. Li, S. Meng, Appl. Phys. Lett. **104**, 131904 (2014)
40. M.-M. Zhang, L. Xu, J. Zhang, J. Phys. Condens. Matter **27**, 445301 (2015)
41. C. Lian, J. Ni, AIP Adv. **3**, 052102 (2013)
42. M.Z. Hasan, C.L. Kane, Rev. Mod. Phys. **82**, 3045 (2010)
43. E. Prada, P. San-Jose, L. Brey, H.A. Fertig, Solid State Commun. **151**, 10751083 (2011)
44. J. Wang, B. Lian, S.-C. Zhang, Phys. Scr. **T164**, 014003 (2015)
45. N.A. Sinitsyn, J.E. Hill, H. Min, J. Sinova, A.H. MacDonald, Phys. Rev. Lett. **97**, 106804 (2006)
46. D.N. Sheng, Z.Y. Weng, L. Sheng, F.D.M. Haldane, Phys. Rev. Lett. **97**, 036808 (2006)
47. Y. Yang, Z. Xu, L. Sheng, B. Wang, D.Y. Xing, D.N. Sheng, Phys. Rev. Lett. **107**, 066602 (2011)